Eur. Phys. J. C 16, 253–267 (2000)
Digital Object Identifier (DOI) 10.1007/s100520000400

THE EUROPEAN PHYSICAL JOURNAL C

Search for resonances decaying to e^+-jet in e^+p interactions at HERA

The ZEUS Collaboration

J. Breitweg, S. Chekanov, M. Derrick, D. Krakauer, S. Magill, B. Musgrave, A. Pellegrino, J. Repond, R. Stanek, R. Yoshida
Argonne National Laboratory, Argonne, IL, USA [p]

M.C.K. Mattingly
Andrews University, Berrien Springs, MI, USA

G. Abbiendi, F. Anselmo, P. Antonioli, G. Bari, M. Basile, L. Bellagamba, D. Boscherini[1], A. Bruni, G. Bruni, G. Cara Romeo, G. Castellini[2], L. Cifarelli[3], F. Cindolo, A. Contin, N. Coppola, M. Corradi, S. De Pasquale, P. Giusti, G. Iacobucci, G. Laurenti, G. Levi, A. Margotti, T. Massam, R. Nania, F. Palmonari, A. Pesci, A. Polini, G. Sartorelli, Y. Zamora Garcia[4], A. Zichichi
University and INFN Bologna, Bologna, Italy [f]

C. Amelung, A. Bornheim, I. Brock, K. Coböken, J. Crittenden, R. Deffner, H. Hartmann, K. Heinloth, E. Hilger, P. Irrgang, H.-P. Jakob, A. Kappes, U.F. Katz, R. Kerger, E. Paul, H. Schnurbusch, A. Stifutkin, J. Tandler, K.Ch. Voss, A. Weber, H. Wieber
Physikalisches Institut der Universität Bonn, Bonn, Germany [c]

D.S. Bailey, O. Barret, N.H. Brook[5], B. Foster[6], G.P. Heath, H.F. Heath, J.D. McFall, D. Piccioni, E. Rodrigues, J. Scott, R.J. Tapper
H.H. Wills Physics Laboratory, University of Bristol, Bristol, UK [o]

M. Capua, A. Mastroberardino, M. Schioppa, G. Susinno
Calabria University, Physics Departmentand INFN, Cosenza, Italy [f]

H.Y. Jeoung, J.Y. Kim, J.H. Lee, I.T. Lim, K.J. Ma, M.Y. Pac[7]
Chonnam National University, Kwangju, Korea [h]

A. Caldwell, W. Liu, X. Liu, B. Mellado, S. Paganis, R. Sacchi, S. Sampson, F. Sciulli
Columbia University, Nevis Labs., Irvington on Hudson, N.Y., USA [q]

J. Chwastowski, A. Eskreys, J. Figiel, K. Klimek, K. Olkiewicz, K. Piotrzkowski[8], M.B. Przybycień, P. Stopa, L. Zawiejski
Inst. of Nuclear Physics, Cracow, Poland [j]

L. Adamczyk, B. Bednarek, K. Jeleń, D. Kisielewska, A.M. Kowal, T. Kowalski, M. Przybycień, E. Rulikowska-Zarębska, L. Suszycki, D. Szuba
Faculty of Physics and Nuclear Techniques, Academy of Mining and Metallurgy, Cracow, Poland [j]

A. Kotański
Jagellonian University, Department of Physics, Cracow, Poland [k]

L.A.T. Bauerdick, U. Behrens, J.K. Bienlein, C. Burgard[9], K. Desler, G. Drews, A. Fox-Murphy,U. Fricke, F. Goebel, P. Göttlicher, R. Graciani, T. Haas, W. Hain, G.F. Hartner, D. Hasell[10], K. Hebbel, K.F. Johnson[11], M. Kasemann[12], W. Koch, U. Kötz, H. Kowalski, L. Lindemann[13], B. Löhr, M. Martínez,M. Milite, T. Monteiro[8], M. Moritz, D. Notz, F. Pelucchi, M.C. Petrucci, M. Rohde, P.R.B. Saull, A.A. Savin, U. Schneekloth, F. Selonke, M. Sievers, S. Stonjek, E. Tassi, G. Wolf, U. Wollmer,
C. Youngman, W. Zeuner
Deutsches Elektronen-Synchrotron DESY, Hamburg, Germany

C. Coldewey, H.J. Grabosch, A. Lopez-Duran Viani, A. Meyer, S. Schlenstedt, P.B. Straub
DESY Zeuthen, Zeuthen, Germany

G. Barbagli, E. Gallo, P. Pelfer
University and INFN, Florence, Italy [f]

G. Maccarrone, L. Votano
INFN, Laboratori Nazionali di Frascati, Frascati, Italy [f]

A. Bamberger, A. Benen, S. Eisenhardt[14], P. Markun, H. Raach, S. Wölfle
Fakultät für Physik der Universität Freiburg i.Br., Freiburg i.Br., Germany [c]

P.J. Bussey, A.T. Doyle, S.W. Lee, N. Macdonald, G.J. McCance, D.H. Saxon, L.E. Sinclair,
I.O. Skillicorn, R. Waugh
Department of Physics and Astronomy, University of Glasgow, Glasgow, UK [o]

I. Bohnet, N. Gendner,U. Holm, A. Meyer-Larsen, H. Salehi, K. Wick
Hamburg University, I. Institute of Exp. Physics, Hamburg, Germany [c]

D. Dannheim, A. Garfagnini, I. Gialas[15], L.K. Gladilin[16], D. Kçira[17], R. Klanner,E. Lohrmann, G. Poelz, F. Zetsche
Hamburg University, II. Institute of Exp. Physics, Hamburg, Germany [c]

R. Goncalo, K.R. Long, D.B. Miller, A.D. Tapper, R. Walker
Imperial College London, High Energy Nuclear Physics Group, London, UK [o]

U. Mallik
University of Iowa, Physics and Astronomy Department, Iowa City, USA [p]

P. Cloth, D. Filges
Forschungszentrum Jülich, Institut für Kernphysik, Jülich, Germany

T. Ishii, M. Kuze, K. Nagano, K. Tokushuku[18], S. Yamada, Y. Yamazaki
Institute of Particle and Nuclear Studies, KEK, Tsukuba, Japan [g]

S.H. Ahn, S.B. Lee, S.K. Park
Korea University, Seoul, Korea [h]

H. Lim, I.H. Park, D. Son
Kyungpook National University, Taegu, Korea [h]

F. Barreiro, G. García, C. Glasman[19], O. Gonzalez, L. Labarga, J. del Peso, I. Redondo[20], J. Terrón
Univer. Autónoma Madrid, Depto de Física Teórica, Madrid, Spain [n]

M. Barbi,F. Corriveau, D.S. Hanna, A. Ochs, S. Padhi, M. Riveline, D.G. Stairs, M. Wing
McGill University, Department of Physics, Montréal, Québec, Canada [a], [b]

T. Tsurugai
Meiji Gakuin University, Faculty of General Education, Yokohama, Japan

V. Bashkirov[21], B.A. Dolgoshein
Moscow Engineering Physics Institute, Moscow, Russia [l]

R.K. Dementiev, P.F. Ermolov, Yu.A. Golubkov, I.I. Katkov, L.A. Khein, N.A. Korotkova,
I.A. Korzhavina, V.A. Kuzmin, O.Yu. Lukina, A.S. Proskuryakov, L.M. Shcheglova, A.N. Solomin,
N.N. Vlasov, S.A. Zotkin
Moscow State University, Institute of Nuclear Physics, Moscow, Russia [m]

C. Bokel,M. Botje, N. Brümmer, J. Engelen, S. Grijpink, E. Koffeman, P. Kooijman, S. Schagen, A. van Sighem,
H. Tiecke, N. Tuning, J.J. Velthuis, J. Vossebeld, L. Wiggers, E. de Wolf
NIKHEF and University of Amsterdam, Amsterdam, The Netherlands [i]

D. Acosta[22],B. Bylsma, L.S. Durkin, J. Gilmore, C.M. Ginsburg, C.L. Kim, T.Y. Ling
Ohio State University, Physics Department, Columbus, Ohio, USA [p]

S. Boogert, A.M. Cooper-Sarkar, R.C.E. Devenish, J. Große-Knetter[23], T. Matsushita, O. Ruske, M.R. Sutton, R. Walczak
Department of Physics, University of Oxford, Oxford UK [o]

A. Bertolin, R. Brugnera, R. Carlin, F. Dal Corso, U. Dosselli, S. Dusini, S. Limentani, M. Morandin, M. Posocco, L. Stanco, R. Stroili, C. Voci
Dipartimento di Fisica dell' Università and INFN, Padova, Italy [f]

L. Iannotti[24], B.Y. Oh, J.R. Okrasiński, W.S. Toothacker, J.J. Whitmore
Pennsylvania State University, Department of Physics, University Park, PA, USA [q]

Y. Iga
Polytechnic University, Sagamihara, Japan [g]

G. D'Agostini, G. Marini, A. Nigro
Dipartimento di Fisica, University 'La Sapienza' and INFN, Rome, Italy [f]

C. Cormack, J.C. Hart, N.A. McCubbin, T.P. Shah
Rutherford Appleton Laboratory, Chilton, Didcot, Oxon, UK [o]

D. Epperson, C. Heusch, H.F.-W. Sadrozinski, A. Seiden, R. Wichmann, D.C. Williams
University of California, Santa Cruz, CA, USA [p]

N. Pavel
Fachbereich Physik der Universität-Gesamthochschule Siegen, Germany [c]

H. Abramowicz[25], S. Dagan[26], S. Kananov[26], A. Kreisel, A. Levy[26]
Raymond and Beverly Sackler Faculty of Exact Sciences, School of Physics, Tel-Aviv University, Tel-Aviv, Israel [e]

T. Abe, T. Fusayasu, K. Umemori, T. Yamashita
Department of Physics, University of Tokyo, Tokyo, Japan [g]

R. Hamatsu, T. Hirose, M. Inuzuka, S. Kitamura[27], T. Nishimura
Tokyo Metropolitan University, Department of Physics, Tokyo, Japan [g]

M. Arneodo[28], N. Cartiglia, R. Cirio, M. Costa, M.I. Ferrero, S. Maselli, V. Monaco, C. Peroni, M. Ruspa, A. Solano, A. Staiano
Università di Torino, Dipartimento di Fisica Sperimentale and INFN, Torino, Italy [f]

M. Dardo
II Faculty of Sciences, Torino University and INFN, Alessandria, Italy [f]

D.C. Bailey, C.-P. Fagerstroem, R. Galea, T. Koop, G.M. Levman, J.F. Martin, R.S. Orr, S. Polenz, A. Sabetfakhri, D. Simmons
University of Toronto, Department of Physics, Toronto, Ont., Canada [a]

J.M. Butterworth,C.D. Catterall, M.E. Hayes, E.A. Heaphy, T.W. Jones, J.B. Lane, B.J. West
University College London, Physics and Astronomy Department, London, UK [o]

J. Ciborowski, R. Ciesielski, G. Grzelak, R.J. Nowak, J.M. Pawlak, R. Pawlak, B. Smalska, T. Tymieniecka, A.K. Wróblewski, J.A. Zakrzewski, A.F. Żarnecki
Warsaw University, Institute of Experimental Physics, Warsaw, Poland [j]

M. Adamus, T. Gadaj
Institute for Nuclear Studies, Warsaw, Poland [j]

O. Deppe, Y. Eisenberg[26], D. Hochman, U. Karshon[26]
Weizmann Institute, Department of Particle Physics, Rehovot, Israel [d]

W.F. Badgett, D. Chapin, R. Cross, C. Foudas, S. Mattingly, D.D. Reeder, W.H. Smith, A. Vaiciulis[29], T. Wildschek, M. Wodarczyk
University of Wisconsin, Department of Physics, Madison, WI, USA [p]

A. Deshpande, S. Dhawan, V.W. Hughes
Yale University, Department of Physics, New Haven, CT, USA [P]

S. Bhadra, C. Catterall, J.E. Cole, W.R. Frisken, R. Hall-Wilton, M. Khakzad, S. Menary, W.B. Schmidke
York University, Department of Physics, Toronto, Ont., Canada [a]

Received: 15 February 2000 / Published online: 18 May 2000 –

Abstract. The e^+-jet invariant mass spectrum produced in the reaction $e^+p \to e^+X$ has been studied at a center-of-mass energy of 300 GeV. The data were collected using the ZEUS detector operating at the HERA collider, and correspond to an integrated luminosity of 47.7 pb^{-1}. The observed mass spectrum is in good agreement with Standard Model expectations up to an e^+-jet mass of 210 GeV. Above this mass, some excess is seen. The angular distribution of these events is typical of high-Q^2 neutral current events and does not give convincing evidence for the presence of a narrow scalar or vector state. Limits are presented on the product of cross section and branching ratio for such a state and are interpreted as limits on leptoquark or R-parity-violating squark production. Specific leptoquark types are ruled out at 95% confidence level for coupling strength $\lambda = 0.3$ for masses between 150 and 280 GeV.

1 Introduction

The e^+-jet mass spectrum in e^+p scattering has been investigated with the ZEUS detector at HERA. An excess of

[1] now visiting scientist at DESY
[2] also at IROE Florence, Italy
[3] now at University of Salerno and INFN Napoli, Italy
[4] supported by Worldlab, Lausanne, Switzerland
[5] PPARC Advanced fellow
[6] also at University of Hamburg, Alexander von Humboldt Research Award
[7] now at Dongshin University, Naju, Korea
[8] now at CERN
[9] now at Barclays Capital PLC, London
[10] now at Massachusetts Institute of Technology, Cambridge, MA, USA
[11] visitor from Florida State University
[12] now at Fermilab, Batavia, IL, USA
[13] now at SAP A.G., Walldorf, Germany
[14] now at University of Edinburgh, Edinburgh, UK
[15] visitor of University of Crete, Greece, partially supported by DAAD, Bonn - Kz. A/98/16764
[16] on leave from MSU, supported by the GIF, contract I-0444-176.07/95
[17] supported by DAAD, Bonn - Kz. A/98/12712
[18] also at University of Tokyo
[19] supported by an EC fellowship number ERBFMBICT 972523
[20] supported by the Comunidad Autonoma de Madrid
[21] now at Loma Linda University, Loma Linda, CA, USA
[22] now at University of Florida, Gainesville, FL, USA
[23] supported by the Feodor Lynen Program of the Alexander von Humboldt foundation
[24] partly supported by Tel Aviv University
[25] an Alexander von Humboldt Fellow at University of Hamburg
[26] supported by a MINERVA Fellowship
[27] present address: Tokyo Metropolitan University of Health Sciences, Tokyo 116-8551, Japan
[28] now also at Università del Piemonte Orientale, I-28100 Novara, Italy
[29] now at University of Rochester, Rochester, NY, USA
[a] supported by the Natural Sciences and Engineering Research Council of Canada (NSERC)
[b] supported by the FCAR of Québec, Canada
[c] supported by the German Federal Ministry for Education and Science, Research and Technology (BMBF), under contract numbers 057BN19P, 057FR19P, 057HH19P, 057HH29P, 057SI75I
[d] supported by the MINERVA Gesellschaft für Forschung GmbH, the German Israeli Foundation, and by the Israel Ministry of Science
[e] supported by the German-Israeli Foundation, the Israel Science Foundation, the U.S.-Israel Binational Science Foundation, and by the Israel Ministry of Science
[f] supported by the Italian National Institute for Nuclear Physics (INFN)
[g] supported by the Japanese Ministry of Education, Science and Culture (the Monbusho) and its grants for Scientific Research
[h] supported by the Korean Ministry of Education and Korea Science and Engineering Foundation
[i] supported by the Netherlands Foundation for Research on Matter (FOM)
[j] supported by the Polish State Committee for Scientific Research, grant No. 112/E-356/SPUB/DESY/P03/DZ 3/99, 620/E-77/SPUB/DESY/P-03/ DZ 1/99, 2P03B03216, 2P03B04616, 2P03B03517, and by the German Federal Ministry of Education and Science, Research and Technology (BMBF)
[k] supported by the Polish State Committee for Scientific Research (grant No. 2P03B08614 and 2P03B06116)
[l] partially supported by the German Federal Ministry for Education and Science, Research and Technology (BMBF)
[m] supported by the Fund for Fundamental Research of Russian Ministry for Science and Education and by the German Federal Ministry for Education and Science, Research and Technology (BMBF)
[n] supported by the Spanish Ministry of Education and Science through funds provided by CICYT
[o] supported by the Particle Physics and Astronomy Research Council
[P] supported by the US Department of Energy
[q] supported by the US National Science Foundation

events relative to Standard Model expectations has previously been reported by the H1 [1,2] and ZEUS [3,4] collaborations in neutral current deep inelastic scattering at high x and high Q^2. These events contain high-mass e^+-jet final states. Several models have been discussed [5] as possible sources of these events, including leptoquark production [6] and R-parity-violating squark production [7]. This paper presents an analysis of ZEUS data specifically aimed at searching for high-mass states decaying to e^+-jet.

Candidate events with high transverse energy, an identified final-state positron, and at least one jet are selected. The measured energies (E'_e, E_j) and angles of the final-state positron and the jet with highest transverse momentum are used to calculate an invariant mass

$$M^2_{ej} = 2E'_e E_j \cdot (1 - \cos\xi) \,, \qquad (1)$$

where ξ is the angle between the positron and jet. The angle between the outgoing and incoming positron in the e^+-jet rest frame, θ^*, is also reconstructed using the measured energies and angles. No assumptions about the production process are made in the reconstruction of either M_{ej} or θ^*.

The search was performed using 47.7 pb^{-1} of data collected in the 1994-1997 running periods. In the following, expectations from the Standard Model, leptoquark production and R-parity-violating squark production are summarized. After a discussion of the experimental conditions, the analysis is described and the M_{ej} and $\cos\theta^*$ distributions presented. Since these distributions do not show a clear signal for a narrow resonance, limits on the cross section times branching ratio are extracted for the production of such a state. Limits are also presented in the mass versus coupling plane which can be applied to leptoquark and squark production.

2 Model expectations

High-mass e^+-jet pairs, produced in the Standard Model (SM) via neutral current (NC) scattering, form the principal background to the search for heavy states. This process is reviewed first. Leptoquark (LQ) production and squark production in R-parity-violating ($\not{R}_P$) supersymmetry are used as examples of physics beyond the SM that could generate the e^+-jet final state. The diagrams for NC and LQ processes are shown in Fig. 1. The squark production diagrams are similar to the LQ diagrams, but different decay modes are possible, as discussed below.

2.1 Standard model expectations

The kinematic variables used to describe the deep inelastic scattering (DIS) reaction

$$e^+p \to e^+X$$

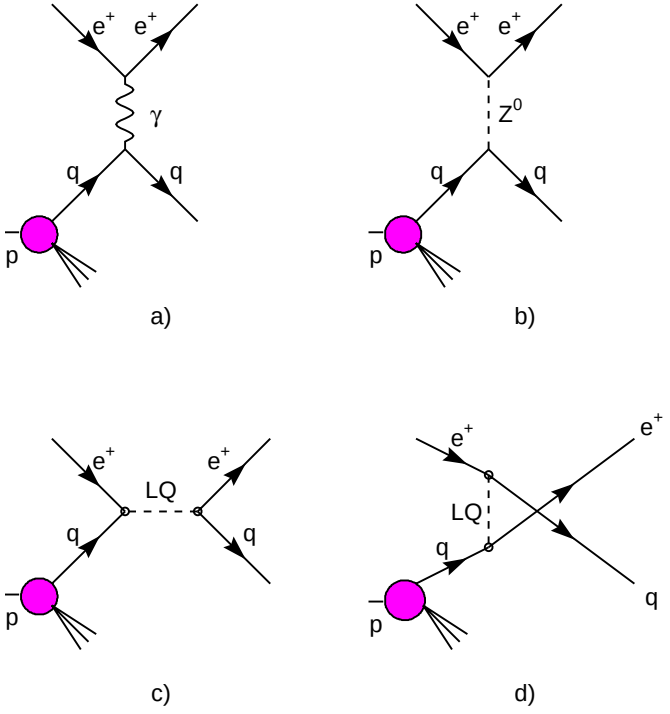

Fig. 1a–d. Diagrams for NC scattering via **a** photon exchange and **b** Z^0 exchange. The leptoquark diagrams for the same initial and final states are **c** s-channel LQ production for fermion number $F = 0$ LQ and **d** u-channel LQ exchange for an $F = 2$ LQ

are

$$Q^2 = -q^2 = -(k - k')^2 \,, \qquad (2)$$

$$y = \frac{q \cdot P}{k \cdot P} \qquad \text{and} \qquad (3)$$

$$x = \frac{Q^2}{2q \cdot P} \,, \qquad (4)$$

where k and k' are the four-momenta of the incoming and outgoing positron, respectively, and P is the four-momentum of the incoming proton. The center-of-mass energy is given by $s = (k + P)^2 \approx (300\ \text{GeV})^2$. The NC interaction occurs between the positron and a parton (quark) inside the proton (see Fig. 1). The production of the large e^+-jet masses of interest requires high-x-partons, where the valence quarks dominate the proton structure.

In leading-order electroweak theory, the cross section for the NC DIS reaction can be expressed as [8]

$$\frac{d^2\sigma(e^+p)}{dxdy} = \frac{2\pi\alpha^2}{sx^2y^2}\left[Y_+F_2 - Y_-xF_3 + y^2F_L\right] \qquad (5)$$

with $Y_\pm = 1 \pm (1-y)^2$ and α the fine structure constant. The contribution from the longitudinal structure function, F_L, is expected to be negligible in the kinematic range considered here.

The x dependence of the NC cross section is very steep. In addition to the explicit $1/x^2$ factor, the structure functions F_2 and xF_3 are dominated at large x by valence-

quark densities that fall quickly for $x > 0.3$. The y dependence of the cross section is dominated by the $1/y^2$ term. The structure functions vary slowly with y at fixed x. The uncertainty in the NC cross section predicted by 5 is dominated by the uncertainty in the structure functions (parton densities), and is small, about 5% at the high-x and moderate-y ranges of this analysis [4]. The quantity of interest in this paper is the e^+-jet cross section, which is sensitive to QCD corrections. The uncertainty arising from these corrections has been estimated to be small for this analysis.

For DIS or LQ events produced via the diagrams shown in Fig. 1 (i.e. assuming no QED or QCD radiation), the mass of the eq system is related to x via

$$M^2 = sx \tag{6}$$

and θ^* is related to y via

$$\cos\theta^* = 1 - 2y\ . \tag{7}$$

The steeply falling x and y dependences of DIS events will therefore produce distributions falling sharply with mass and peaking towards $\cos\theta^* = 1$.

2.2 Leptoquark production and exchange

Leptoquark production is an example of new physics that could generate high-mass e^+-jet pairs. The set of leptoquarks with $SU(3) \times SU(2) \times U(1)$-invariant couplings has been specified [6]. Only LQs with fermion number $F = L + 3B = 0$ are considered here, where L and B denote the lepton and baryon number, respectively. These leptoquarks are listed in Table 1 together with some of their properties. The $F = 0$ LQs have higher cross sections in e^+p scattering than e^-p scattering since in the e^+p case a valence quark can fuse with the positron.

In principle, additional LQ types can be defined [9] which depend on the generations of the quarks and leptons to which they couple. Only LQs which preserve lepton flavor and couple to first-generation quarks are considered in this analysis.

As shown in Fig. 1, leptoquark production can generate an s-channel resonance provided $m_{LQ} < \sqrt{s}$. Contributions to the e^+p cross section would also result from u-channel exchange and interference of LQ diagrams with photon and Z^0 exchange. The cross section in the presence of a leptoquark can be written as

$$\frac{d^2\sigma(e^+p)}{dxdy} = \frac{d^2\sigma^{NC}}{dxdy} + \frac{d^2\sigma^{Int}_{u/NC}}{dxdy} + \frac{d^2\sigma^{Int}_{s/NC}}{dxdy} + \frac{d^2\sigma^{LQ}_{u}}{dxdy} + \frac{d^2\sigma^{LQ}_{s}}{dxdy}\ . \tag{8}$$

The first term on the right-hand side of 8 represents the SM contribution discussed previously. The second (third) term arises from the interference between the SM and u-channel (s-channel) LQ diagram, and the fourth (fifth) term represents the u-channel (s-channel) LQ diagram alone. The additional contributions to the SM cross section depend on two parameters: m_{LQ}, and λ_R or λ_L, the coupling to $e^+_{L,R}$ and quark. Leptoquarks of well-defined helicity ($\lambda_R \cdot \lambda_L = 0$) are assumed for simplicity in the limit-setting procedure, and one species of LQ is assumed to dominate the cross section. The $\cos\theta^*$ dependence varies strongly for the different terms: it is flat for scalar-LQ production in the s channel, and for vector-LQ exchange in the u channel, while it varies as $(1+\cos\theta^*)^2$ for vector-LQ production in the s channel or scalar-LQ exchange in the u channel. The interference terms produce a $\cos\theta^*$ dependence which is steeper due to the sharply peaking $\cos\theta^*$ distribution in NC DIS.

In general, the s-channel term dominates the additional contributions to the SM cross section if $m_{LQ} < \sqrt{s}$, the coupling λ is small, and the LQ is produced from a quark rather than an antiquark. However, there are conditions for which the other terms can become significant, or even dominant [11], leading to important consequences for the expected mass spectra and decay angular distributions. The u-channel and interference terms cannot produce a resonance peak in the mass spectrum and the angular distributions from such terms can behave more like those of NC deep inelastic scattering. Limits are presented in this paper for narrow-width LQ and under conditions for which the s-channel term dominates.

Table 1. The $F = 0$ leptoquarks that can be produced at HERA. The LQ species are divided according to their spin (S for scalar and V for vector), their chirality (L or R) and their weak isospin $(0, 1/2, 1)$. The leptoquarks $\tilde{S}$ and $\tilde{V}$ differ by two units of hypercharge from S and V, respectively. In addition, the electric charge, q, of the leptoquarks, the production channel, as well as their allowed decay channels assuming lepton-flavor conservation, are displayed. The quantum numbers and decay channels correspond to an electron-type LQ. For positrons, the corresponding anti-leptoquarks have the sign of the electric charge reversed, the helicity of the incoming lepton reversed and antiquarks are replaced by the corresponding quark. The nomenclature follows the Aachen convention [10]

LQ species	q	Production	Decay	Branching ratio
$S^L_{1/2}$	-5/3	$e_L\bar{u}$	$e\bar{u}$	1
$S^R_{1/2}$	-5/3	$e_R\bar{u}$	$e\bar{u}$	1
	-2/3	$e_R\bar{d}$	$e\bar{d}$	1
$\tilde{S}^L_{1/2}$	-2/3	$e_L\bar{d}$	$e\bar{d}$	1
V^L_0	-2/3	$e_L\bar{d}$	$e\bar{d}$	1/2
			$\nu_e\bar{u}$	1/2
V^R_0	-2/3	$e_R\bar{d}$	$e\bar{d}$	1
$\tilde{V}^R_0$	-5/3	$e_R\bar{u}$	$e\bar{u}$	1
V^L_1	-5/3	$e_L\bar{u}$	$e\bar{u}$	1
	-2/3	$e_L\bar{d}$	$e\bar{d}$	1/2
			$\nu_e\bar{u}$	1/2

The width of a LQ depends on its spin and decay modes, and is proportional to m_{LQ} times the square of the coupling. In the narrow-width approximation, the LQ production cross section is given by integrating the s-channel term [6]:

$$\sigma^{NWA} = (J+1)\frac{\pi}{4s}\lambda^2 q(x_0,\mu) \quad (9)$$

where J represents the spin of the LQ, $q(x_0,\mu)$ is the quark density evaluated at $x_0 = m_{LQ}^2/s$ and with the scale $\mu = m_{LQ}^2$. In the limit-setting procedure (Sect. 8), this cross section was corrected for expected QED and QCD (for scalar LQ only) radiative effects. The QCD corrections [12] enhance the cross section by 20 - 30% for the $F = 0$ LQ considered here. The effect of QED radiation on the LQ production cross section was calculated and was found to decrease the cross section by 5-25% as m_{LQ} increases from $100 \to 290$ GeV.

2.3 R-parity-violating squark production

In the supersymmetry (SUSY) superpotential, R-parity-violating terms of the form $\lambda'_{ijk} L_L^i Q_L^j \overline{D}_R^k$ [7] are of particular interest for lepton-hadron collisions. Here, L_L, Q_L, and $\overline{D}_R$ denote left-handed lepton and quark doublets and the right-handed down-type quark-singlet chiral superfields, respectively. The indices i, j, and k label their respective generations.

For $i = 1$, which is the case for ep collisions, these operators can lead to $\tilde{u}$- and $\tilde{d}$-type squark production. There are 9 possible production couplings probed in e^+p collisions, corresponding to the reactions [13]

$$e^+ + \bar{u}_j \to \tilde{\bar{d}}_k \ , \quad (10)$$

$$e^+ + d_k \to \tilde{u}_j \ . \quad (11)$$

For production and decay via the λ'_{1jk} coupling, squarks behave like scalar leptoquarks and the final state is indistinguishable, event by event, from Standard Model neutral and charged current events. However, as for the scalar leptoquarks, the angular distributions of the final-state lepton and quark will be different and this fact can be exploited in performing searches. Limits derived for scalar LQ production can then be directly related to limits on squark production and decay via λ'_{ijk}. In addition to the Yukawa couplings, gauge couplings also exist whereby $\tilde{q}$ can decay by radiating a neutralino or chargino which can subsequently decay. The final-state signature depends on the properties of the neutralino or chargino. The search for such decay topologies from a squark is outside the scope of this analysis.

3 Experimental conditions

In 1994-97, HERA operated with protons of energy $E_p = 820$ GeV and positrons of energy $E_e = 27.5$ GeV. The ZEUS detector is described in detail elsewhere [14]. The main components used in the present analysis were the central tracking detector (CTD) positioned in a 1.43 T solenoidal magnetic field and the uranium-scintillator sampling calorimeter (CAL). The CTD was used to establish an interaction vertex with a typical resolution along (transverse to) the beam direction of 0.4 (0.1) cm. It was also used in the positron-finding algorithm that associated a charged track with an energy deposit in the calorimeter. The CAL was used to measure the positron and hadronic energies. The CAL consists of a forward part (FCAL), a barrel part (BCAL) and a rear part (RCAL), with depths of 7, 5 and 4 interaction lengths, respectively. The FCAL and BCAL are segmented longitudinally into an electromagnetic section (EMC), and two hadronic sections
(HAC1,2). The RCAL has one EMC and one HAC section. The cell structure is formed by scintillator tiles; cell sizes range from 5×20 cm^2 (FEMC) to 24.4×35.2 cm^2 at the front face of a BCAL HAC2 cell. The light generated in the scintillator is collected on both sides of the module by wavelength-shifter bars, allowing a coordinate measurement based on knowledge of the attenuation length in the scintillator. The light is converted into an electronic signal by photomultiplier tubes. The cells are arranged into towers consisting of 4 EMC cells, a HAC1 cell and a HAC2 cell (in FCAL and BCAL). The transverse dimensions of the towers in FCAL are 20×20 cm^2. One tower is absent at the center of the FCAL and RCAL to allow space for passage of the beams. The outer boundary of the inner ring of FCAL towers, used to define a fiducial cut for the jet reconstruction, defines a box of 60×60 cm^2.

Under test beam conditions, the CAL has energy resolutions of $\sigma/E = 0.18/\sqrt{E}$ for positrons hitting the center of a calorimeter cell and $\sigma/E = 0.35/\sqrt{E}$ for single hadrons, where energies are in GeV. In the ZEUS detector, the energy measurement is affected by the energy loss in the material between the interaction point and the calorimeter. For the events selected in this analysis, the positrons predominantly strike the BCAL, while the jets hit the FCAL. The in-situ positron-energy resolution in the BCAL has been determined to average $\sigma/E = 0.32/\sqrt{E} \oplus 0.03$ while the jet-energy resolution in the FCAL averages $\sigma/E = 0.55/\sqrt{E} \oplus 0.02$. The jet-energy resolution was determined by comparing reconstructed jet energies in the calorimeter with the total energy of the particles in the hadronic final-state using Monte Carlo simulation, and therefore includes small contributions from the jet-finding algorithm.

In the reconstruction of the positron and jet energies, corrections were applied for inactive materials located in front of the calorimeter and for non-uniformities in the calorimeter response [4]. For the high energies important in this analysis, the overall energy scale is known to 1% for positrons in BCAL and 2% for hadrons in FCAL and BCAL. The electromagnetic energy scale was determined by a comparison with momentum measurements in the central tracking detector (using lower-energy electrons and positrons). Its linearity was checked with energies reconstructed from the double angle (DA) method [15]. The

hadronic-energy scales in the FCAL and BCAL were determined by using transverse-momentum balance in NC DIS events.

The angular reconstruction was performed using a combination of tracking and calorimeter information. From Monte Carlo studies, the polar-angle resolutions were found to be 2.5 mrad for positrons and approximately $(220/\sqrt{E}-4)$ mrad for jets with energies above 100 GeV.

The luminosity was measured from the rate of the bremsstrahlung process $e^+p \to e^+p\gamma$ [16], and has an uncertainty of 1.6%.

The ZEUS coordinate system is right-handed and centered on the nominal interaction point, with the Z axis pointing in the direction of the proton beam (forward) and the X axis pointing horizontally toward the center of HERA. The polar angle θ is defined with respect to the Z axis.

4 Event selection

The events of interest with large e^+-jet mass contain a final-state positron at a large angle and of much higher energy than that of the incident positron beam, as well as one or more energetic jets. The only important SM source of such events is NC scattering with large Q^2. Other potential backgrounds, such as high transverse-energy (E_T) photoproduction, were determined to be negligible.

The following requirements selected events of the desired topology:

- A reconstructed event vertex was required in the range $|Z| < 50$ cm.
- The total transverse energy, E_T, was required to be at least 60 GeV.
- An identified [4] positron was required with energy $E'_e > 25$ GeV, located either in the FCAL or BCAL. The positron was required to be well-contained in the BCAL or FCAL and not to point to the BCAL/FCAL interface, at approximately $31^\circ < \theta < 36^\circ$. Positrons within 1.5 cm of the boundary between adjacent BCAL modules, as determined by tracking information, were also discarded to remove showers developing in the wavelength-shifter bars.
- A hadronic jet with transverse momentum $P_T^j > 15$ GeV, located in a region of good containment, was required. The jets were reconstructed using the longitudinally invariant k_T-clustering algorithm [17] in the inclusive mode [18]. Only jets with a reconstructed centroid outside the inner ring of FCAL towers were considered. In events where multiple jets were reconstructed, the jet with highest transverse momentum was used. After all cuts, 12% of the events had more than one jet, both in the data and Monte Carlo simulation (see below).

The E_T cut, the jet-containment cut and the positron-containment cut define the available kinematic region for further analysis, as shown in Fig. 2. The jet containment cut, in particular, limits the values of $\cos\theta^*$ that can be measured at the highest e^+-jet masses. Because most such events have $\cos\theta^*$ near 1, the acceptance for NC DIS events (with $E_T > 60$ GeV) falls below 10% for masses beyond 220 GeV. In the region allowed by the cuts shown in Fig. 2, the acceptance is typically 80%.

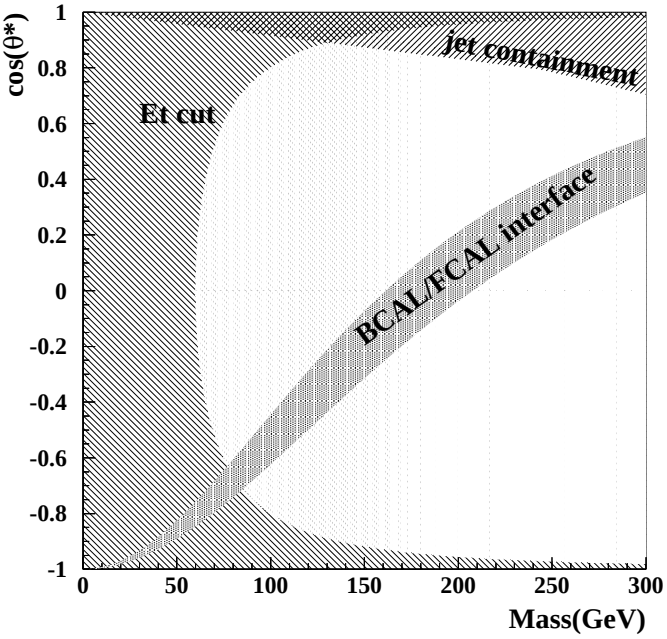

Fig. 2. The acceptance region (unshaded) in the $\cos\theta^*$ versus M_{ej} plane allowed by the E_T, jet-containment and positron-fiducial-volume cuts, assuming $eq \to eq$ scattering at the nominal interaction point. No detector simulation is included

A total of 7103 events remained after applying all cuts, compared to 6949 ± 445 events predicted by the NC Monte Carlo simulation based on the measured luminosity of 47.7 pb^{-1} (the sources of uncertainty on the expected number of events are described in Sect. 7.1). The E_T distributions for data and NC simulation are compared in Fig. 3a. The positron transverse-momentum (P_T^e) spectrum, jet transverse-momentum (P_T^j) spectrum and the ratio P_T^e/P_T^h, where P_T^h is the transverse momentum of the hadronic system, are shown in Figs. 3(b-d), respectively. The missing transverse momentum, $\not{P}_T$, and the longitudinal momentum variable, $E - P_Z$, are compared in Figs. 3(e,f). The global properties of the events are well reproduced by the simulation.

5 Event simulation

The SM deep inelastic scattering events were simulated using the HERACLES 4.5.2 [19] program with the DJANGO 6 version 2.4 [20] interface to the hadronization programs. In HERACLES, corrections for initial- and final-state electroweak radiation, vertex and propagator corrections, and two-boson exchange are included. The NC DIS hadronic final state was simulated using the MEPS model of LEPTO 6.5 [21], which includes order α_S matrix elements and models of higher-order QCD radiation. As a systematic check, the NC final state was simulated using the color-

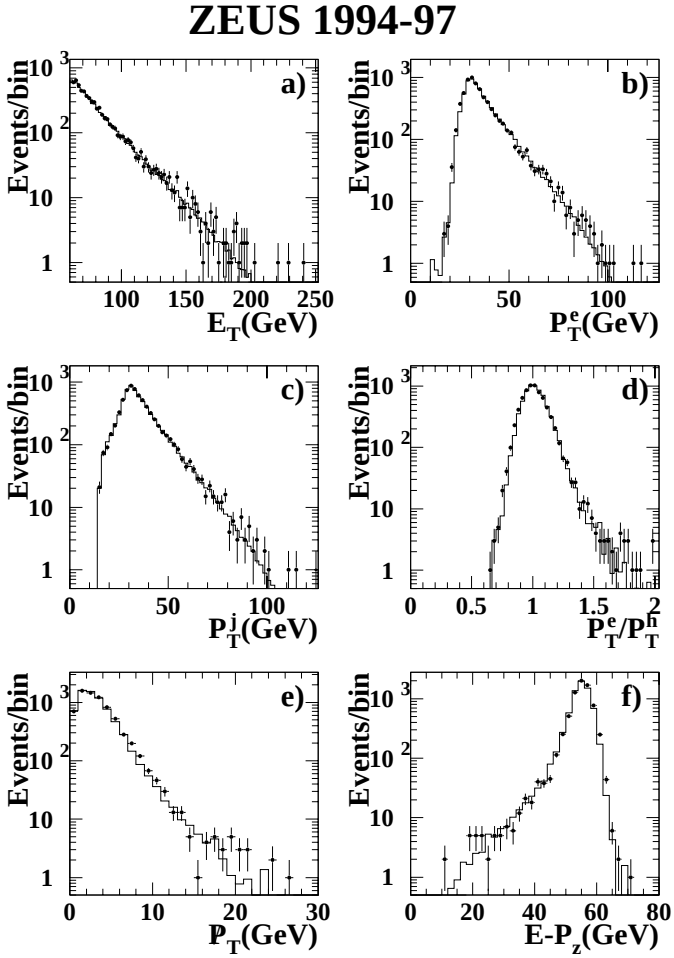

Fig. 3a–f. Comparison of data (points) with Standard Model expectations (histograms) for selected distributions: **a** total transverse energy, E_T; **b** positron transverse momentum, P_T^e; **c** jet transverse momentum, P_T^j; **d** the ratio of the positron to hadron transverse momenta, P_T^e/P_T^h, **e** the missing transverse momentum, $\not{P}_T$, and **f** the longitudinal-momentum variable, $E - P_Z$, for the event

dipole model of ARIADNE 4.08 [22]. The CTEQ4 parton-distribution set [23] was used to evaluate the expected number of events from NC DIS scattering.

The leptoquark events were generated using PYTHIA 6.1 [24]. This program takes into account the finite width of the LQ, but only includes the s-channel diagrams. Initial- and final-state QCD radiation from the quark and the effect of LQ hadronization before decay are taken into account, as are initial- and final-state QED radiation from the positron.

The generated events were input into a GEANT-based [25] program which simulated the response of the ZEUS detector. The trigger and offline processing requirements applied to the data were applied to the simulated events. The luminosity of the NC Monte Carlo samples ranges from 46 pb^{-1} at $Q^2 = 400$ GeV^2 to $7.3 \cdot 10^6$ pb^{-1} at $Q^2 = 50000$ GeV^2.

6 Mass and θ^* reconstruction

The mass of each e^+-jet pair was reconstructed from the measured energies and angles of the positron and jet as described by 1. This formula makes no correction for the finite jet mass. Possible mass shifts and the resolutions for resonant lepton-hadron states were estimated from PYTHIA. Narrow scalar LQ events in the mass range $150 - 290$ GeV were simulated. The mean mass for reconstructed events was found to be within 6% of the generated value, while the peak position as determined by a Gaussian fit was typically lower than the generated value by only 1%. The average mass resolution, determined from a Gaussian fit to the peak of the reconstructed mass spectrum, ranged from 5.5% to 3% for masses from 150 to 290 GeV. The RMS of the distribution was typically twice as large.

The positron scattering angle in the e^+-jet rest frame, θ^*, was reconstructed as the angle between the incoming and outgoing positron directions in this frame. These directions were determined by performing a Lorentz transformation using the measured positron and jet energies and angles in the laboratory frame. The resolution in $\cos\theta^*$ near $|\cos\theta^*| = 1$, as determined from a Gaussian fit, was near 0.01, degrading to 0.03 as $|\cos\theta^*|$ decreases. The shift in $\cos\theta^*$ was less than 0.01 for both the NC MC and the leptoquark MC.

In order to determine limits on leptoquark and squark production, the mass of the electron-hadron system was reconstructed by the constrained-mass method. This method reconstructs the e^+-hadron mass as

$$M_{CJ} = \sqrt{2E_e(E + P_Z)} \qquad (12)$$

where $(E + P_Z)$ is the sum of the energy and P_Z contributions from the positron and all jets satisfying $P_T^j > 15$ GeV and pseudorapidity $\eta_j < 3$ (with the highest P_T jet required to be outside the FCAL inner ring). The η_j cut removes contributions from the proton remnant. The constraints $\not{P}_T = 0$ and $E - P_Z = 2E_e$, which are satisfied by fully contained events, have been assumed in arriving at this equation. When using this mass-reconstruction method, events with measured $E - P_Z < 40$ GeV were removed to avoid large initial-state QED radiation.

The M_{CJ} method gave, on average, improved resolution over the M_{ej} method for narrow LQ MC events. The improved resolution occurred at smaller $\cos\theta^*$ (for $\cos\theta^* \approx 0$ the mass resolution determined from a Gaussian fit to the reconstructed mass distribution for $m_{LQ} = 200$ GeV was about 1.5% in the M_{CJ} method and 3% for the M_{ej} method); at the larger $\cos\theta^*$ values where NC DIS events are concentrated, the resolutions of the two methods were similar (about 3% for $m_{LQ} = 200$ GeV). The M_{CJ} method relies on constraints which do not necessarily apply to a resonant state whose properties cannot be anticipated in detail. We therefore choose to use the M_{ej} method as our primary search method. The M_{CJ} method is used in the limit-setting procedure.

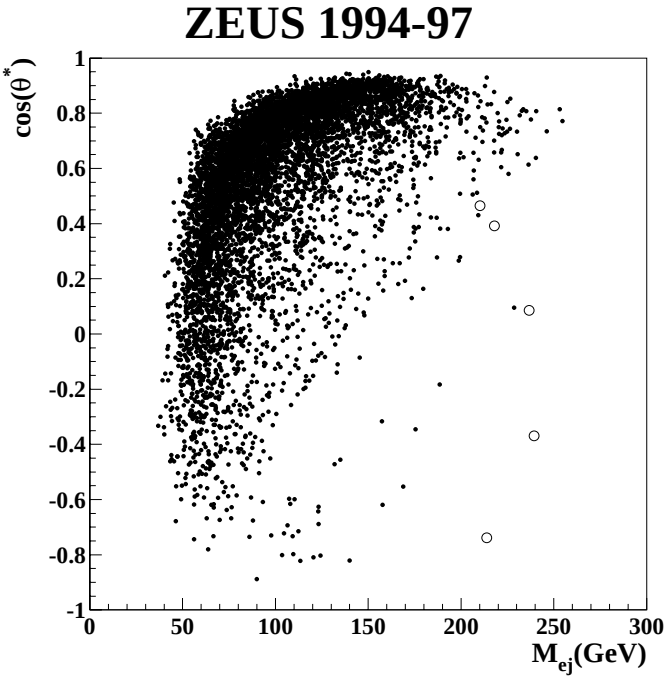

Fig. 4. The value of $\cos\theta^*$ versus M_{ej} for all 7103 events passing the event selections. The events at high x and y described in a previous paper [3] are shown as open circles

7 M_{ej} and $\cos\theta^*$ distributions

The reconstructed values of M_{ej} are plotted versus $\cos\theta^*$ for the selected events in Fig. 4. Most of the events are concentrated at large $\cos\theta^*$ and small mass, as expected from Standard Model NC scattering. The five events indicated as open circles are from data taken in 1994-96, with total luminosity 20 pb^{-1}. They were the subject of a previous publication [3]. In this earlier analysis, the kinematic variables were reconstructed with the DA method. The five events also stand out with the M_{ej} reconstruction technique. The average value of M_{ej} for these events is 224 GeV, or 7 GeV less than the corresponding mass calculated previously via $M = \sqrt{s \cdot x_{DA}}$, where x_{DA} is the estimator of Bjorken-x calculated with the DA method. This mass shift is compatible with expectations based on resolution and initial state radiation effects. With the present luminosity of 47.7 pb^{-1}, 7 events are observed in the region of $M_{ej} > 200$ GeV and $\cos\theta^* < 0.5$, where 5.0 events are expected.

The M_{ej} spectrum for events with $M_{ej} > 100$ GeV is shown in Fig. 5a on a logarithmic scale. The high-mass part of the spectrum is shown on a linear scale in the inset. The predicted number of events (N^{pred}) from NC processes is shown as the histogram. The ratio of the measured mass spectrum to the expectation is shown in Fig. 5b. The shaded band indicates the systematic uncertainty on the expectations.

7.1 Systematic uncertainties

The uncertainty on N^{pred} varies with mass from 7% at 100 GeV up to 30% at 250 GeV. The most important uncertainties are on the energy scale and the jet position. The NC DIS cross section given in 5 (neglecting F_L) can be rewritten in terms of the e^+q invariant mass, M, and the polar angle of the outgoing struck quark in the laboratory frame, γ:

$$\frac{d^2\sigma(e^+p)}{dMd\gamma} = \frac{32\pi\alpha^2 E_e^2 \sin\gamma}{M^5(1-\cos\gamma)^2}\left[Y_+F_2 - Y_-xF_3\right] \quad . \qquad (13)$$

The mass dependence is very steep. In addition to the explicit M^{-5} dependence, there is also a strong suppression of high masses implicit in the structure functions. An incorrect energy scale will produce a shift in the mass spectrum and potentially a significant error in the number of expected events at a given mass. The dependence on the quark angle is also steep, approximately γ^{-3} at small γ. The number of events passing the jet fiducial cut is therefore strongly dependent on the accuracy of the jet position reconstruction. The jet fiducial-volume cut requires the highest-P_T jet to point outside the inner ring of FCAL towers. Many distributions from data and MC were compared to search for possible systematic biases.

The dominant sources of uncertainty are itemized below in order of decreasing importance:

1. Knowledge of the calorimeter energy scales:
   The scale uncertainties discussed in Sect. 3 are 1% for BCAL positrons and 2% for hadrons, leading to an uncertainty of 5(18)% in N^{pred} at $M_{ej} = 100(210)$ GeV.
2. Uncertainties in the simulation of the hadronic energy flow, including simulation of the proton remnant, the energy flow between the struck quark and proton remnant, and possible detector effects in the innermost calorimeter towers:
   Many distributions of data and MC were compared and no important systematic differences were found. Figure 6 shows the fraction of the jet energy in the inner ring of FCAL towers associated with the highest P_T jet as a function of η_j. This is shown for all events in Fig. 6a, as well as for those with $M_{ej} > 210$ GeV in Fig. 6b. For the highest η_j values considered, this ratio is about 20%. The energy located in the innermost towers of the FCAL and not associated with the highest P_T jet is shown in Fig. 6c,d, and compared to the MC simulation. No large differences are seen between data and MC (the lowest η bin in Fig 6d contains only five data events). The innermost towers of the FCAL have a larger uncertainty in the energy scale than the rest of the FCAL owing to their slightly different construction and proximity to the beam. The energy in these cells has been varied by ±10%. As a test of the simulation of the forward energy flow, the ARIADNE MC has been used instead of the LEPTO MC. These tests yielded variations in N^{pred} of 13% at $M_{ej} = 210$ GeV.

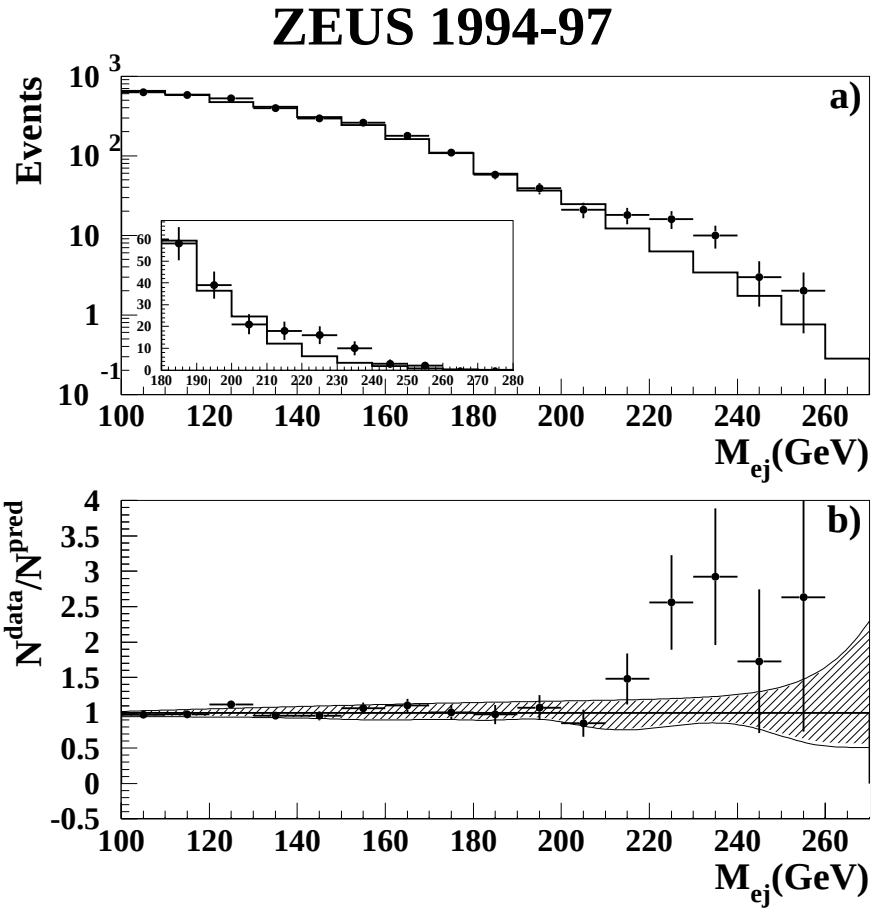

Fig. 5. a Comparison of observed events (points) and SM expectations (histogram) for the reconstructed e^+-jet invariant mass. The inset shows the region with $M_{ej} > 180$ GeV on a linear scale. **b** The ratio of the number of observed events to the Standard Model expectations. The shaded band shows the systematic uncertainty in the predicted number of events. The error bars on the data points are calculated from the square root of the number of events in the bin

3. Uncertainty in the parton density functions:
   The parton density functions were estimated as in [4], and led to an uncertainty of 5% in N^{pred} at $M_{ej} =$ 210 GeV.
4. Uncertainties in the acceptance:
   The alignment of the FCAL was determined to better than 5 mm, and various jet position reconstruction algorithms were compared. These studies yielded an uncertainty of 2% in N^{pred}.
5. Uncertainties in the energy resolution functions:
   These were studied by comparing tracking information with calorimeter information for individual events, as well as by comparing different reconstruction methods. The MC energies were smeared by additional amounts to represent these uncertainties, leading to a variation of less than 5% in N^{pred}.

Other uncertainties include positron finding efficiency, luminosity determination, vertex simulation, multijet production rates, and hadronization simulation. These were found to be small in comparison to the items listed above. The overall systematic uncertainty was obtained by summing the contributions from all these sources in quadrature.

7.2 Discussion

The data in Fig. 5 are in good agreement with the SM expectations up to $M_{ej} \approx 210$ GeV. Some excess is seen at higher masses. For $M_{ej} > 210$ GeV, 49 events were observed in the data, while 24.7 ± 5.6 events are expected. A careful study of individual events in this mass region uncovered no signs of reconstruction errors. Rather, the events always contain clear examples of a high-energy positron (typically 70 GeV) near 90° and a high-energy jet (typically 400 GeV) in the forward direction (2 events have a second jet, in accord with NC DIS Monte Carlo expectations). The distributions shown in Fig. 3 for all the data are restricted to the events with $M_{ej} > 210$ GeV in Fig. 7. Whereas the shapes of the distributions are similar, the data lie systematically above the MC, which is normalized to the integrated luminosity.

The events with large M_{ej} have characteristics similar on average to NC DIS events. In particular, the $\cos\theta^*$ projection of the events with $M_{ej} > 210$ GeV is shown in Fig. 8 and compared to the MC expectations for neutral current DIS (solid histogram). The expectations for narrow s-channel scalar- and vector-LQ production are also shown for comparison. For $F = 0$ LQs with $\lambda < 1$, the u-channel and interference terms would not significantly affect these expectations. The shape of the data and NC MC $\cos\theta^*$ distributions are qualitatively similar, peaking at high values of $\cos\theta^*$.

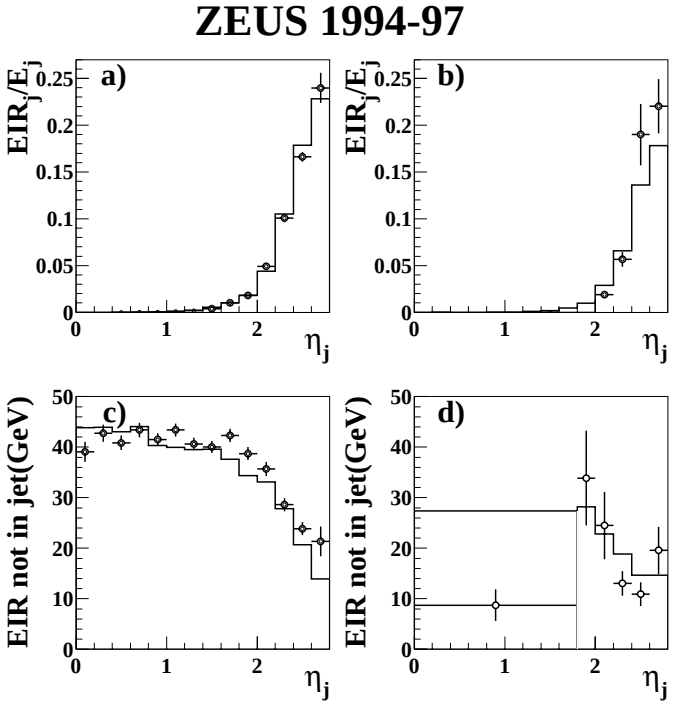

Fig. 6a–d. The ratio of the jet energy in the innermost towers of the FCAL, EIR_j, to the total jet energy, E_j, as a function of η of the jet for **a** the full sample, and **b** for those events with $M_{ej} > 210$ GeV. The energy deposited in the innermost FCAL towers, excluding that associated with the highest P_T jet, is shown in **c** for the full sample, and in **d** for those events with $M_{ej} > 210$ GeV. The data are shown as points, while the NC Monte Carlo predictions are shown as a histogram

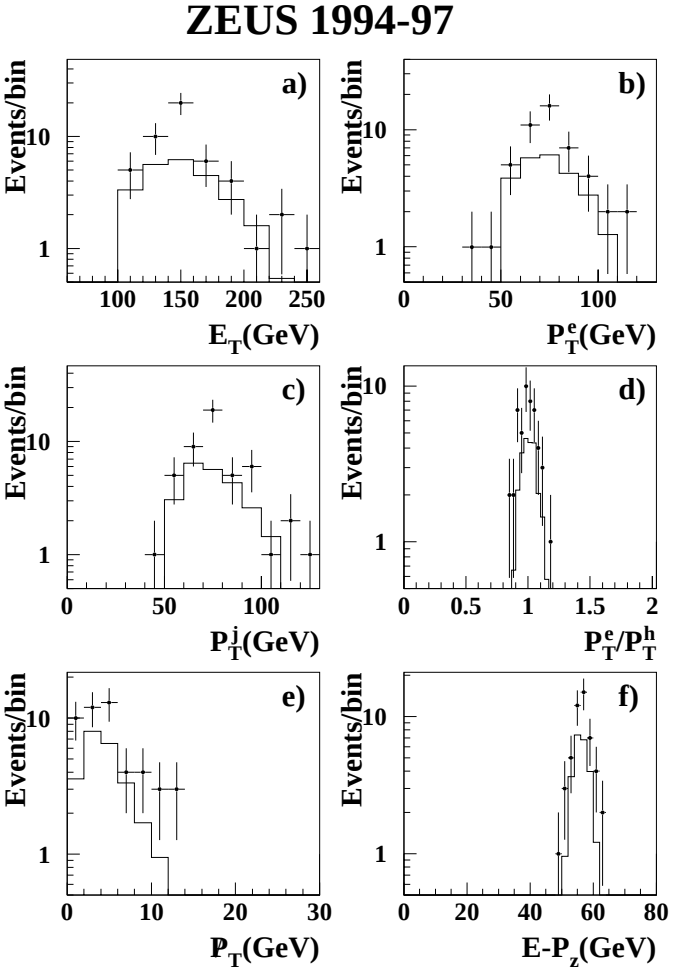

Fig. 7a–f . Comparison of data (points) with Standard Model expectations (histograms) for selected distributions and requiring $M_{ej} > 210$ GeV: **a** total event transverse energy, E_T; **b** positron transverse momentum, P_T^e; **c** jet transverse momentum, P_T^j; **d** the ratio of the positron to hadron transverse momenta, P_T^e/P_T^h, **e** the net (or missing) transverse momentum, $\not{P}_T$, and **f** the longitudinal momentum variable, $E - P_Z$, for the event

In summary, there is some excess of events with $M_{ej} > 210$ GeV above the Standard Model predictions. The probability of observing such an excess depends strongly on possible systematic biases. The most important of these are biases in the energy scales. As a test, many MC experiments were generated where the jet energy scale was shifted by +2% and the electron energy scale by +1%. A window of width $3\sigma(M_{ej})$, where $\sigma(M_{ej})$ is the mass resolution at mass M_{ej}, was moved over the accessible mass range. For each simulated experiment, the number of observed events within the mass window was compared with the nominal expectations as a function of M_{ej}, seeking the excess which gave the largest statistical significance. The same procedure was applied to the data. As a result, it was found that 5% of the simulated experiments would observe, somewhere in the mass spectrum, an excess of statistical significance at least as large as the one found in the data. The excess is therefore not statistically compelling. Furthermore, the events have the characteristics of neutral current scattering. Limits are therefore set on the production of narrow scalar or vector states, as discussed below.

8 Limits on narrow scalar and vector states

Limits are set on the production cross section times branching ratio into positron+jet, σB, for a narrow scalar or vector state. For definiteness, limits on coupling strength versus mass for $F = 0$ leptoquarks are presented, as well as limits on $\lambda\sqrt{B}$ versus mass for scalar states coupling to u or d quarks, such as $\not{R}_P$ squarks. The limits are extracted for $\lambda \leq 1$, allowing the use of the narrow-width approximation assumed in 9.

The M_{CJ} mass reconstruction method was used to set limits as described in Sect. 6. The positron fiducial cuts were removed since this method is less sensitive to the positron-energy measurement, while the cut $E - P_Z > 40$ GeV was applied to reduce radiative effects. The mass spectrum reconstructed with this technique is shown in Fig. 9a. In total, 8026 events passed all selection cuts while 7863 events are predicted by the MC.

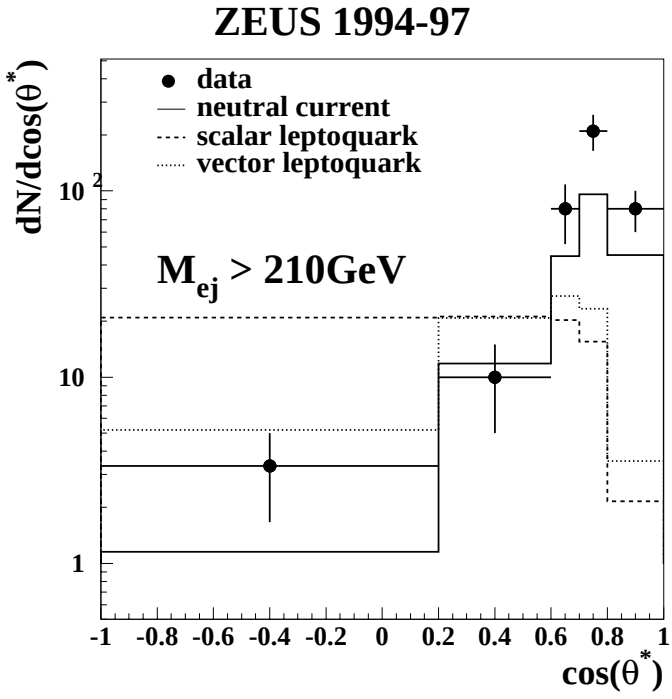

Fig. 8. Comparison of data (points) and NC Monte Carlo expectations (solid histogram) for the $\cos\theta^*$ distribution for events with $M_{ej} > 210$ GeV. The predictions for narrow scalar and vector resonant leptoquarks are shown with arbitrary normalization for comparison

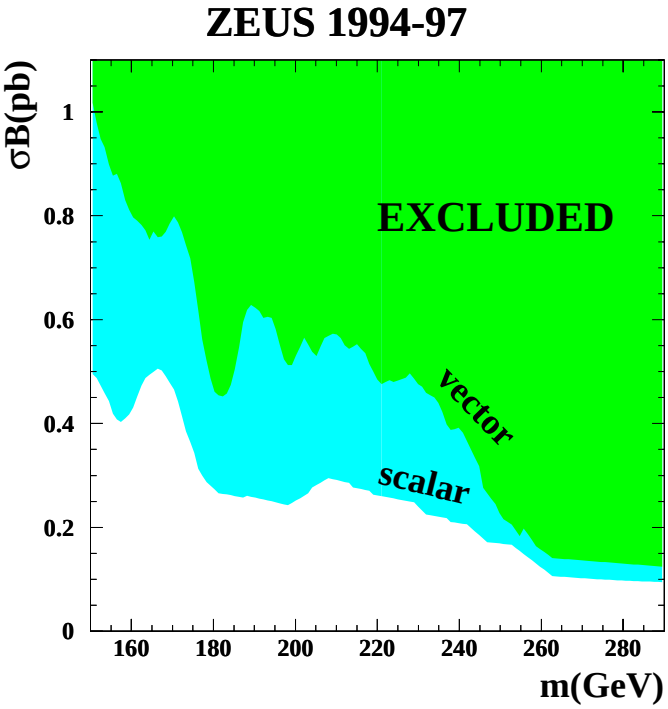

Fig. 10. Limits on the production cross section times branching ratio for decay into e^+-jet(s) for a scalar or vector state, as a function of the mass of the state. The shaded regions are excluded

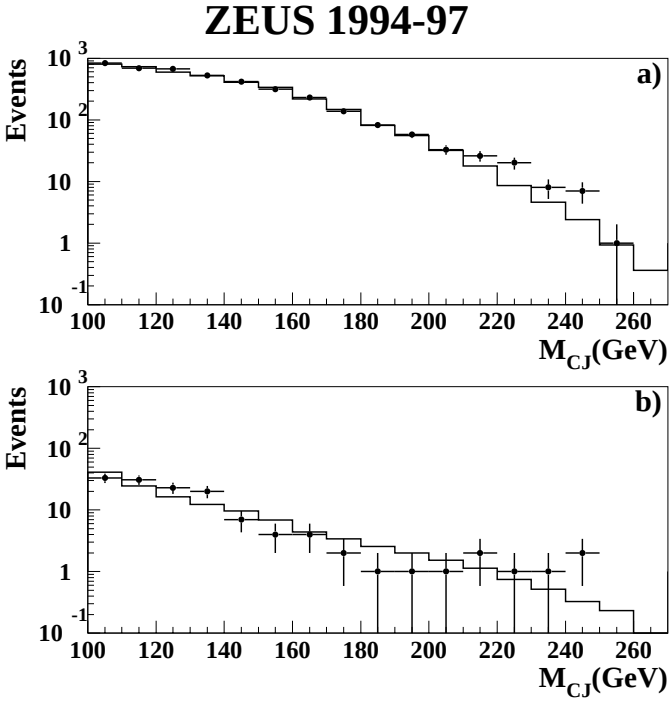

Fig. 9a,b. The reconstructed mass spectrum using the M_{CJ} method for data (points) and SM expectations (histogram): **a** shows the spectrum for events satisfying all cuts, while **b** shows the mass spectrum after the cut ($\cos\theta^* < \cos\theta^*_{cut}$) for the scalar LQ search has been applied

The leptoquark MC described in Sect. 5 was used to determine the event selection efficiency and the acceptance of the fiducial cuts, as well as to estimate the mass resolution. This MC and the NC background simulation were used to calculate an optimal bin width, ΔM_{CJ}, for each M_{CJ}, and optimal $\cos\theta^*$ range, $\cos\theta^* < \cos\theta^*_{cut}$, to obtain on average the best limits on LQ couplings. The bin widths were typically 20 GeV. The values of $\cos\theta^*_{cut}$ for setting limits range from 0.5 to 0.9 for vector leptoquarks with masses between 150−290 GeV, and from 0.1 to 0.9 for scalar leptoquarks in the same mass range. The mass spectrum after applying the optimal $\cos\theta^*$ cut for the scalar search is shown in Fig. 9b. No significant deviations from expectations are seen after applying this cut.

The 95% confidence level (CL) limits on σB were obtained directly from the observed number of data events with $\cos\theta^* < \cos\theta^*_{cut}$ in the particular mass window [26]. The procedure described in [26] was extended to include the systematic uncertainties in the numbers of predicted events. This was found to have negligible effect on the limits. The limits for a narrow scalar or vector state are shown in Fig. 10. These limits lie between 1 and 0.1 pb as the mass increases from 150 to 290 GeV.

The 95% CL exclusion limits for different species of LQ are given in the coupling versus mass plane in Fig. 11. The limits exclude leptoquarks with coupling strength $\lambda = \sqrt{4\pi\alpha} \approx 0.3$ for masses up to 280 GeV for specific types of F=0 leptoquarks. The H1 collaboration has recently published similar limits [2]. In Fig. 11, the ZEUS results are compared to recent limits from OPAL. At LEP [27–

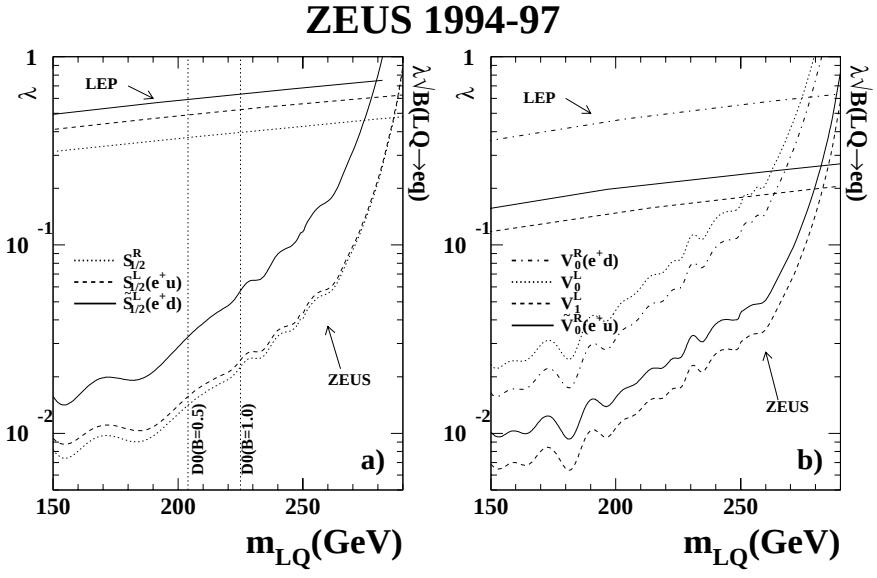

Fig. 11a,b. Coupling limits as a function of leptoquark mass for $F = 0$ leptoquarks. The results from this analysis are compared to representative limits from LEP [28] and the Tevatron [31]. The areas above the ZEUS and LEP curves are excluded, while the area to the left of the Tevatron line is excluded for scalar leptoquarks with the indicated branching ratio to e+jet. The limits on scalars are shown in **a** while the limits on vectors are shown in **b**

29], sensitivity to a high-mass LQ arises from effects of virtual LQ exchange on the hadronic cross section. The HERA and LEP limits are complementary to Tevatron limits [30,31], which are independent of the coupling $\lambda_{L,R}$. The limits by D0 (CDF) extend up to 225 (213) GeV for a scalar LQ with 100% branching ratio to eq. The D0 limits are shown as vertical lines in Fig. 11. The Tevatron limits for vector LQs are model dependent [32], but are expected to be considerably higher than for scalar LQs.

The ZEUS limits presented in Fig. 11 can also be applied to any narrow state which couples to a positron and a u or d quark and with unknown branching ratio to e^+-jet(s). These states correspond to the leptoquark types as labelled in the figure. For these states, the limits are on the quantity $\lambda\sqrt{B}$. Examples of scalar states for which these limits apply are $\not{R}_P$ squarks (e.g.,the limit on the $\tilde{S}^L_{1/2}(e^+d)$ LQ can be read as a limit on the λ'_{1j1} R-parity-violating coupling).

9 Conclusion

Data from 47.7 pb^{-1} of e^+p collisions at a center-of-mass energy of 300 GeV have been used to search for a resonance decaying into e^+-jet. The invariant mass of the e^+-jet pair was calculated directly from the measured energies and angles of the positron and jet. This approach makes no assumptions about the production mechanism of such a state.

The observed mass spectrum is in good agreement with Standard Model expectations up to e^+-jet masses of about 210 GeV. Above this mass, some excess is seen. The angular distribution of these events is typical of high-Q^2 neutral current events and does not give convincing evidence for the presence of a narrow scalar or vector state. By applying restrictions on the decay angle to optimize sensitivity to a narrow state in the presence of NC background, limits have been derived on the cross section times decay branching fraction for a scalar or vector state decaying into positron and jet(s). These limits can be interpreted, for example, as limits on leptoquark or R-parity-violating squark production. Limits on the production of leptoquarks and squarks are presented in the coupling strength versus mass plane. At a coupling strength $\lambda = 0.3$, new states are ruled out at 95% confidence level for masses between 150 and 280 GeV.

Acknowledgements. We thank the DESY Directorate for their strong support and encouragement, and the HERA machine group for their diligent efforts. We are grateful for the support of the DESY computing and network services. The design, construction and installation of the ZEUS detector have been made possible by the ingenuity and effort of many people from DESY and home institutes who are not listed as authors. It is also a pleasure to thank W. Buchmüller, R. Rückl and M. Spira for useful discussions.

References

1. H1 Collab., C. Adloff et al., Z. Phys. C74 191 (1997); H1 Collab., DESY 99-107, Accepted by Eur. Phys. J. C
2. H1 Collab., C. Adloff et al., Eur. Phys. J. C11 447 (1999) and erratum ibid
3. ZEUS Collab., J. Breitweg et al., Z. Phys. C74 207 (1997)
4. ZEUS Collab., J. Breitweg et al., Eur. Phys. J. C11 427 (1999)
5. Yu. L. Dokshitzer, Proc. of the 5th International Workshop on Deep Inelastic Scattering and QCD, Chicago, IL, USA, Eds. J. Repond and D. Krakauer, American Institute of Physics (1997)
6. W. Buchmüller, R. Rückl and D. Wyler, Phys. Lett. B191 442 (1987); erratum Phys. Lett. B448 320 (1999)
7. J. Butterworth and H. Dreiner, Nucl. Phys. B397 3 (1993), and references therein
8. G. Ingelman and R. Rückl, Phys. Lett. B201 369 (1988)
9. S. Davidson, D. Bailey and B. Campbell, Z. Phys. C61 613 (1994)

10. B. Schrempp, Proc. of the Workshop "Physics at HERA", vol. 1, Eds. W. Buchmüller and G. Ingelman, DESY 1034 (1991)
11. T. Matsushita, E. Perez and R. Rückl, Proc. of the 3rd UK Phenomenology Workshop on HERA Physics, Durham, England (1998), J. Phys. G25 1418 (1999)
12. T. Plehn, H. Spiesberger, M. Spira and P. M. Zerwas, Z. Phys. C74 611 (1997);
Z. Kunszt and W. J. Stirling, Z. Phys. C75 453 (1997)
13. J. L. Hewett, 'Single squark production at HERA via R parity violating interactions', Proc. of the 1990 DPF Summer Study on High-Energy Physics, Snowmass, Colorado, USA, Eds. E. Berger, World Scientific (1992)
14. ZEUS Collab., "The ZEUS Detector", Status Report 1993, DESY 1993
15. S. Bentvelsen, J. Engelen and P. Kooijman, Proc. of the Workshop "Physics at HERA", vol. 1, Eds. W. Buchmüller and G. Ingelman, DESY 23 (1991) ; K. C. Hoeger, ibid. 43
16. J. Andruszków et al., DESY 92-066 (1992); ZEUS Collab., M. Derrick et al., Z. Phys. C63 391 (1994)
17. S. Catani, Yu. L. Dokshitzer, M. H. Seymour and B. R. Webber, Nucl. Phys. B406 187 (1993)
18. S. D. Ellis and D. E. Soper, Phys. Rev. D48 3160 (1993)
19. HERACLES 4.4: A. Kwiatkowski, H. Spiesberger and H.-J. Möhring, Comput. Phys. Commun. 69 155 (1992)
20. DJANGO 1: K. Charchula, G. A. Schuler and H. Spiesberger, Comput. Phys. Commun. 81 381 (1994)
21. LEPTO 6.1: G. Ingelman, A. Edin and J. Rathsman, Comput. Phys. Commun. 101 108 (1997)
22. ARIADNE 4: L. Lönnblad, Comput. Phys. Commun. 71 15 (1992)
23. CTEQ Collab., H. L. Lai et al., Phys. Rev. D55 1280 (1997)
24. PYTHIA 6.1, C. Friberg, E. Norrbin and T. Sjöstrand, Phys. Lett. B403 329 (1997)
25. GEANT 3.13: R. Brun et al., CERN-DD/EE/84-1 (1987)
26. Particle Data Group, K. Hikasa et al., Phys. Rev. D45 S1 (1992)
27. L3 Collab., M. Acciarri et al., Phys. Lett. B433 163 (1998)
28. OPAL Collab., G. Abbiendi et al., Eur. Phys. J. C6 1 (1999)
29. ALEPH Collab., R. Barate et al., hep-ex/9904011
30. CDF Collab., F. Abe et al., Phys. Rev. Lett. 79 4327 (1997)
31. D0 Collab., B. Abbott et al., Phys. Rev. Lett. 80 2051 (1998)
32. J. Blümlein, E. Boos and A. Kryukov, Z. Phys. C76 137 (1997)